JOURNAL OF GEOPHYSICAL RESEARCH, VOL. 113, C04020, doi:10.1029/2007JC004347, 2008

The seasonal pCO_2 cycle at 49°N/16.5°W in the northeastern Atlantic Ocean and what it tells us about biological productivity

A. Körtzinger,[1] U. Send,[2] R. S. Lampitt,[3] S. Hartman,[3] D. W. R. Wallace,[1] J. Karstensen,[1] M. G. Villagarcia,[4] O. Llinás,[4] and M. D. DeGrandpre[5]

Received 18 May 2007; revised 1 October 2007; accepted 14 January 2008; published 17 April 2008.

[1] A 2-year record of mixed layer measurements of CO_2 partial pressure (pCO_2), nitrate, and other physical, chemical, and biological parameters at a time series site in the northeast Atlantic Ocean (49°N/16.5°W) is presented. The data show average undersaturation of surface waters with respect to atmospheric CO_2 levels by about 40 ± 15 μatm, which gives rise to a perennial CO_2 sink of 3.2 ± 1.3 mol m^{-2} a^{-1}. The seasonal pCO_2 cycle is characterized by a summer minimum (winter maximum), which is due to the dominance of biological forcing over physical forcing. Our data document a rapid transition from deep mixing to shallow summer stratification. At the onset of shallow stratification, up to one third of the mixed layer net community production during the productive season had already been accomplished. The combination of high prestratification productivity and rapid onset of stratification appears to have caused the observed particle flux peak early in the season. Mixed layer deepening during fall and winter reventilated CO_2 from subsurface respiration of newly exported organic matter, thereby negating more than one third of the carbon drawdown by net community production in the mixed layer. Chemical signatures of both net community production and respiration are indicative of carbon overconsumption, the effects of which may be restricted, though, to the upper ocean. A comparison of the estimated net community production with satellite-based estimates of net primary production shows fundamental discrepancies in the timing of ocean productivity.

Citation: Körtzinger, A., U. Send, R. S. Lampitt, S. Hartman, D. W. R. Wallace, J. Karstensen, M. G. Villagarcia, O. Llinás, and M. D. DeGrandpre (2008), The seasonal pCO_2 cycle at 49°N/16.5°W in the northeastern Atlantic Ocean and what it tells us about biological productivity, *J. Geophys. Res.*, *113*, C04020, doi:10.1029/2007JC004347.

1. Introduction

[2] Understanding and predicting the consequences of and feedbacks to global climate change in the anthropocene world is one of the major challenges of Earth sciences. From an oceanographic perspective, future ocean change will have many facets which require a wide range of observatories and platforms stretching from the seafloor to the atmosphere and from the submeter to the global scale. The highly coupled nature of processes in the ocean calls for comprehensive approaches that combine physical, chemical and biological parameters. As one prominent approach, Eulerian (i.e., fixed point) time series observations have contributed considerably to our understanding of ocean biogeochemistry and biology [e.g., *Steinberg et al.*, 2001]. Among the many lessons learned from time series such as the Bermuda Atlantic Time series (BATS) or the Hawaii Ocean Time series (HOT) is the importance of a sustained long-term multidisciplinary approach.

[3] Despite the recognition of their scientific importance long-term time series have remained few owing to the major efforts involved in the upkeep of such field projects. Recognizing the need for new multidisciplinary long-term ocean observatories, the European funded ANIMATE consortium (Atlantic Network of Interdisciplinary Moorings and Time series for Europe, http://www.noc.soton.ac.uk/animate) set out in 2002 to establish new sites in the North Atlantic. Of these, the PAP site on the Porcupine Abyssal Plain (49°N/16.5°W) is the focus of the present study. A major goal at this site, which is part of the OceanSITES initiative (http://www.oceansites.org), was to observe the seasonal cycle of pCO_2 and its interannual variability and to

[1] Leibniz-Institut für Meereswissenschaften (IFM-GEOMAR), Kiel, Germany.
[2] Scripps Institution of Oceanography, University of California, San Diego, La Jolla, California, USA.
[3] Ocean Biogeochemistry and Ecosystems Research Group, National Oceanography Centre, Southampton, UK.
[4] Instituto Canario de Ciencias Marinas, Telde, Gran Canaria, Spain.
[5] Department of Chemistry, University of Montana, Missoula, Montana, USA.

0148-0227/08/2007JC004347$09.00

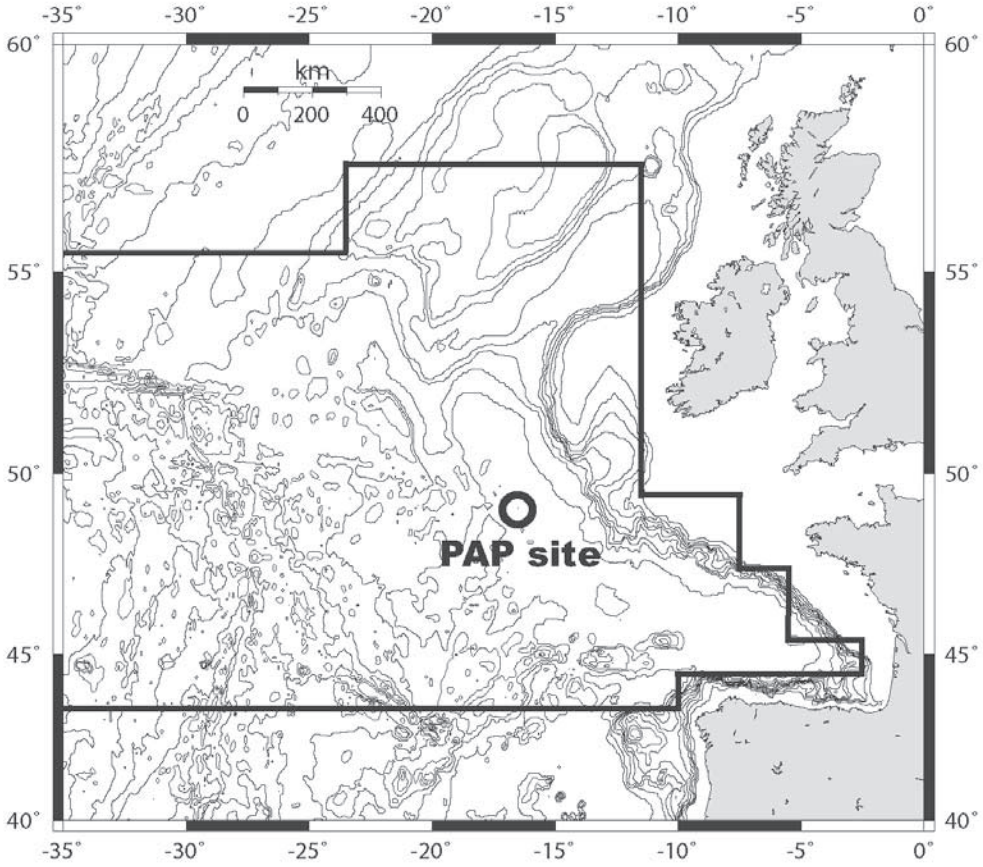

Figure 1. Map of the northeast Atlantic Ocean with the location of the Porcupine Abyssal Plain (PAP) Observatory at 49°N/16.5°W and the boundaries of the North Atlantic Drift Province according to *Longhurst* [2007]. The bathymetry contour interval is 500 m.

deconvolute its physical and biological drivers. Here we present a 2-year data record from this site.

2. Methods and Data

2.1. Porcupine Abyssal Plain Observatory (PAP)

[4] A long-term ocean observatory for physical and biogeochemical observations has been operated since the early 1990s in the northeast Atlantic Ocean at a site in the centre of the approximately 4800 m deep Porcupine Abyssal Plain (49°N/16.5°W, Figure 1) [*Lampitt et al.*, 2001] (http://www.noc.soton.ac.uk/obe/PROJECTS/pap). The site lies in the middle of a biogeochemical province, the North Atlantic Drift Province (NADR) of *Longhurst* [2007], and is characterized by deep winter mixing with strong interannual variability (300–800 m). Furthermore it is located about 350 km to the northeast of the site of the 1989 JGOFS North Atlantic Bloom Experiment (NABE) which has lead to a series of publications (see special section ''JGOFS North Atlantic Bloom Experiment (NABE)'' in *Deep-Sea Research, Part II, 40*(1–2), 641 pp., 1993). Long before NABE, the North Atlantic spring bloom, which is among the largest mass greenings observed on the Earth [*Siegel et al.*, 2002], already fascinated oceanographers [e.g., *Sverdrup*, 1953]. Now, for the first time, continuous measurements of CO_2 partial pressure (pCO_2) and nitrate are available at the PAP site from multidisciplinary moorings supported in part by the European research projects ANIMATE and MERSEA (Marine Environment and Security for the European Area). Data presented here were acquired during three consecutive mooring deployments at PAP between July 2003 and July 2005 (Table 1). All biogeochemical sensors were installed in common sensor frames that were deployed at depths of 23–33 m. Since all

Table 1. Mooring Deployments at the Porcupine Abyssal Plain (PAP) Site (49°N/16.5°W) and Availability of Data

Deployment ID	Date of Deployment	Date of Recovery	Duration, days	Available Parameters
PAP 2	12 Jul 2003	16 Nov 2003	127	T, S, pCO_2, nitrate, chlorophyll *a*, particle flux
PAP 3	17 Nov 2003	16 Jun 2004	212	T, S, pCO_2, nitrate, chlorophyll *a*, particle flux
PAP 4	22 Jun 2004	18 Jul 2005	391	T, S, pCO_2,[a] nitrate,[a] chlorophyll *a*, particle flux

[a]Data record ends before end of deployment.

Table 2. Approximate Deployment Depths (Sampling Intervals) of Moored Instruments From Which Data Have Been Used in This Study

Parameter	PAP 2	PAP 3	PAP 4
Temperature	33 m (15 min)	10 m, 24 m (15 min)	23 m[a] (15 min)
Pressure	33 m (15 min)	10 m, 24 m (15 min)	23 m (15 min)
pCO_2	33 m (1 hour)	24 m (2 hours)	23 m[b] (2 hours)
Nitrate	33 m (8 hours)	24 m (8 hours)	23 m (8 hours)
Chlorophyll *a*	33 m (2 hours)	24 m (2 hours)	23 m[c] (2 hours)
Particle flux	3095 m (14–28 days)	3095 m (14–28 days)	3308 m (14–42 days)

[a]T/S sensor at 10 m depth lost after a few days into the deployment.
[b]Bad data after 17 March 2005.
[c]Bad data after 8 March 2005.

moorings were of subsurface type, this was the closest to the surface the instrument package could be deployed safely.

2.2. Measurements

[5] A suite of physical (temperature, salinity, pressure) and biogeochemical parameters (pCO_2, nitrate, chlorophyll *a*, particle flux) were measured successfully with autonomous instrumentation during the three consecutive deployments presented here (Table 2). Our analysis is restricted to those deployments where pCO_2 data have been successfully acquired (PAP 2–4, Table 2). The pCO_2 sensors of preceding and following PAP deployments were physically destroyed or lost during deployment, respectively.

[6] The pCO_2 was measured with an autonomous sensor (SAMI-CO_2, Sunburst Sensors LLC, Missoula, Montana, USA) which is based on equilibration of a pH indicator solution contained in a gas-permeable membrane with ambient pCO_2 and subsequent spectrophotometric pH determination in the equilibrated solution [*DeGrandpre et al.*, 1995]. The sensor head was covered with a copper mesh to prevent biofouling on all deployments. Nitrate was measured with the NAS-2E in situ wet chemical nutrient analyzer (EnviroTech LLC, Chesapeake, Virginia, USA) using classical wet chemistry protocols. The calibration procedure included a multistandard predeployment laboratory calibration and regular measurements of a blank and two standard solutions throughout the entire deployment. The HydroScat-2 in situ fluorometer with copper shutter for biofouling prevention (Hobi Labs Inc., Tucson, Arizona) was used to measure chlorophyll *a*. Fluorescence data were calibrated against bottle chlorophyll *a* data from hydrocasts with the fluorometers attached to the CTD. Measurements of temperature (T), salinity (S) and pressure were performed with SBE-37 MicroCAT recorders (Sea-Bird Electronics Inc., Bellevue, Washington). In addition, PARFLUX Mark 78 H-21 sediment traps (McLane Research Laboratories Inc., East Falmouth, Massachusetts) were employed to collect particles at a 3000 m nominal depth.

[7] When possible, samples for dissolved inorganic carbon (DIC) and total alkalinity (A_T) were taken from hydrocasts made at the PAP site before deployment or recovery of a mooring for postcalibration of the SAMI-CO_2 sensors (see section 2.3). These samples were measured onshore by extraction and subsequent coulometric titration of the evolved CO_2 for DIC [*Johnson et al.*, 1993] and by open-cell potentiometric seawater titration for A_T [*Mintrop et al.*, 2000]. Accuracy of both DIC and A_T was assured by referencing against certified reference material (CRM) provided by Andrew Dickson (Scripps Institution of Oceanography, La Jolla, California, USA). The corresponding pCO_2 was calculated from measured DIC and A_T at in situ temperature and pressure using the CO2SYS program [*Lewis and Wallace*, 1998] with the constants of *Mehrbach et al.* [1973] as refitted by *Dickson and Millero* [1987].

2.3. Calibration of pCO_2 Data

[8] The SAMI-CO_2 sensors were calibrated by the manufacturer to the expected annual variability range in temperature and pCO_2 and should thus be calibration free on the user side. Also SAMI-CO_2 sensors have been shown on various occasions to exhibit good long-term stability [*DeGrandpre et al.*, 1995, 1999]. However, post calibration of field data sometimes turns out to be necessary to account for problems with the initial calibration (possibly due to changes occurring during sensor shipment) or from drift. In this study, checking and revising factory calibrations proved somewhat difficult and had to be based on different lines of evidence.

[9] First, pCO_2 values calculated from DIC and A_T (see section 2.2) measured on samples from hydrocasts carried out at the mooring site can be employed to postcalibrate pCO_2 sensor readings whereat matching via temperature is preferable to pressure. This method was used whenever possible (PAP 2: start and end of deployment, PAP 3: start of deployment). Uncertainty in these comparisons arises from spatial variability (surface water patchiness), internal wave action (vertical displacement of water properties) and temporal mismatch, i.e., in the timing of the hydrocast and the availability of stable sensor readings at depth. This method was not available at the end of the PAP 4 deployment since the pCO_2 sensor started to malfunction about 4 months before recovery. At the end of the PAP 3/start of the PAP 4 deployment, DIC/A_T samples were taken and analyzed. Calculated pCO_2 values from these samples are deemed to be unreliable, however, as they show high scatter and yield values above 400 μatm which are not to be expected at all in this region during summer and are more than 100 μatm above the sensor values. The cause of this problem was not due to analytical problems but most likely improper poisoning.

[10] Second, when this method failed, plausibility checks were made with underway pCO_2 measurements made on the volunteer observing ship M/V *Falstaff* when passing through the region. Unfortunately no such passage was available during our three consecutive mooring deployments. There are three cruises, however, which passed

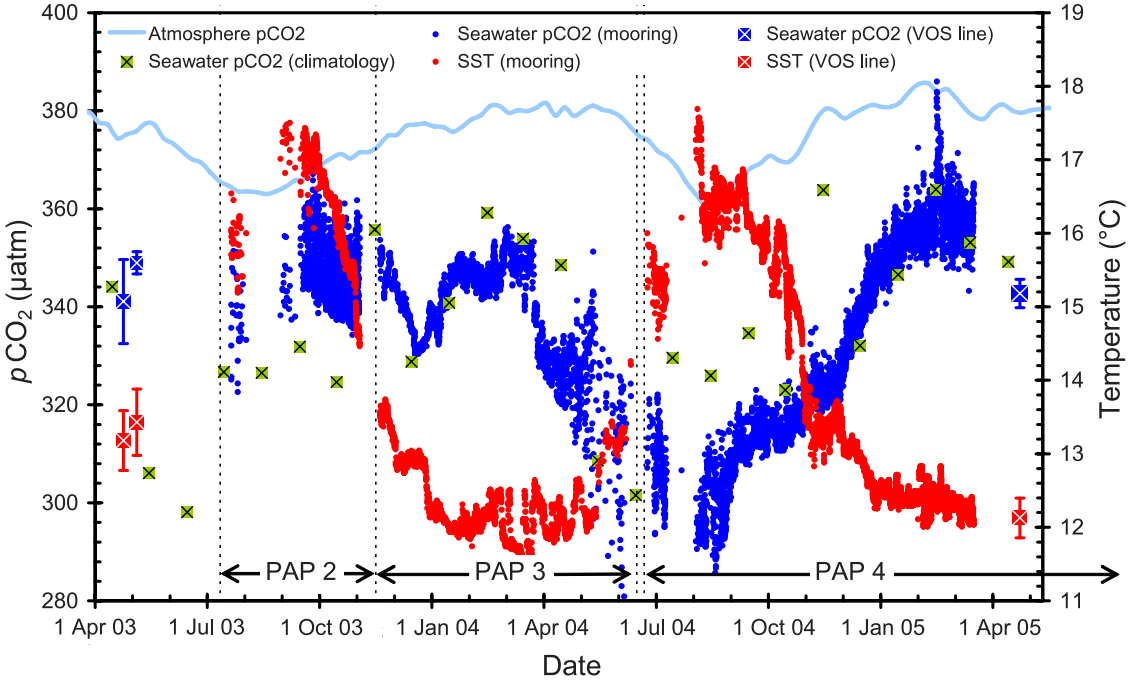

Figure 2. Mixed layer time series of pCO_2 and temperature measured during three consecutive mooring deployments at the PAP site (PAP 2–4, deployment periods indicated by dashed vertical lines). For comparison, pCO_2 and temperature data from a volunteer observing vessel passing through the region are shown, as is the climatological pCO_2 of *Takahashi et al.* [2002], corrected to the time and barometric pressure of the observational period. In addition, the atmospheric pCO_2 at barometric pressure is provided (from GLOBALVIEW-CO_2).

within 150–430 km (Figure 2) of the PAP site either before (April and May 2003, data available via CarboOcean data portal: http://dataportal.carboocean.org) or after the deployment series (T. Steinhoff, IFM-GEOMAR, Kiel, unpublished data, 2005). Of these, the April 2005 cruise lends much credibility to the sensor data which end about one month earlier but are in good agreement, especially when accounting for the seasonal cycle of climatological pCO_2 (Figure 2) [*Takahashi et al.*, 2002].

[11] The postcalibration proved very necessary with the PAP 2 deployment where an offset of +47.5 μatm had to be added at the start of the deployment period which decreased to +33.5 μatm at its end. This offset was varied linearly with time and added to measured pCO_2. The sensor deployed at PAP 3 required an offset correction of +19 μatm at the beginning. Owing to lack of a calibration check at the end of the PAP 3 deployment this time-invariant offset was applied to the entire PAP 3 pCO_2 record. For the PAP 4 pCO_2 record no postcalibration is available. The fact that the PAP 4 record is nicely bracketed on both ends by the calibrated PAP 3 and VOS line data indicate that this sensor did not show a major offset or drift problem.

[12] Taking in account all sources of uncertainty, i.e., uncertainty in calculated pCO_2 due to errors in DIC and A_T as well as in the carbonic acid dissociation constants used, uncertainty from imperfect spatial and temporal match of discrete and VOS line data with the time series record, the overall accuracy of pCO_2 data is likely not better than 5–10 μatm at a precision of about 1 μatm.

2.4. Sources of Ancillary Data

[13] In the present analysis we made use of various other sources of information (Table 3) for the following parameters: sea surface temperature (SST), sea level barometric pressure (SLP), wind speed at 10 m height, atmospheric CO_2 concentration, climatological surface ocean pCO_2 and total alkalinity. Where available, data were retrieved for the pixel (or average of pixels) that represents the location of the PAP site (49°N/16.5°W).

[14] We used the extended CO_2 record derived from continuous measurements at Mace Head, Ireland (53.33°N/9.90°W) to calculate atmospheric pCO_2 at barometric pressure (28-day running mean of 6-hourly SLP, Table 3) and 100% humidity (derived from 28-day running mean of AMSR-E SST, Table 3).

[15] Climatological surface ocean pCO_2 data were retrieved for the PAP site from the *Takahashi et al.* [2002] climatology. As the climatology's reference year is 1995, a correction to our 2003–2005 observation period was necessary. For this the increase of the annual mean atmospheric CO_2 mole fraction at the Mace Head Observatory (Table 3) relative to 1995 was added to the 1995 climatological pCO_2 for the PAP site pixel. This correction assumes that the ocean follows the atmospheric CO_2 level with a disequilibrium that is not changing with time. This may not be exactly the case in reality but the currently available information does not provide a quantitatively consistent picture for a different correction.

[16] Mixed layer depths were estimated from vertical temperature and salinity profiles measured by ARGO floats

Table 3. Sources of Ancillary Data Used in the Present Study

Parameter	Source
Sea surface temperature	Advanced Microwave Scanning Radiometer (AMSR-E) on NASA EOS Aqua satellite, level-3 daily product in 0.25° by 0.25° resolution [*Wentz and Meissner*, 2004]
Barometric pressure	FNMOC 1° by 1° 6-hourly sea level pressure, PFEL live access server, http://www.pfeg.noaa.gov/products/las.html
Vertical T/S profiles	ARGO float observatory, ARGO GDAC, Global Ocean Data Assimilation Experiment, http://www.usgodae.org
10-m wind speed	FNMOC 1° by 1° 6-hourly wind field, PFEL live access server, http://www.pfeg.noaa.gov/products/las.html
Atmospheric CO_2	GLOBALVIEW-CO_2, Cooperative Atmospheric Data Integration Project [*GLOBALVIEW-CO_2*, 2006], http://www.cmdl.noaa.gov/ccgg/globalview/co2/
Surface ocean pCO_2	Climatology for reference year 1995 [*Takahashi et al.*, 2002]
Surface ocean alkalinity	Global Surface Ocean Alkalinity Climatology, calculated using regional A_T relationships [*Lee et al.*, 2006] and monthly mean SST/SSS fields from the *World Ocean Atlas 2001*, http://cdiac.ornl.gov/oceans/Lee_Surface_Alk_Climatol.html
Chlorophyll *a*	MODIS Aqua level-3 standard chlorophyll product, http://oceancolor.gsfc.nasa.gov/
Net primary production	Ocean Productivity Web site with VGPM and CbPM products, http://web.science.oregonstate.edu/ocean.productivity/index.php

within 300 km of the PAP site. We calculated mixed layer depths with the temperature and the density criteria of *de Boyer Montégut et al.* [2004]. These define the base of the mixed layer by a temperature or density difference relative to the surface of −0.2°C and 0.03 kg m^{-3}, respectively. We herein always use the mean of the two estimates.

3. Results and Discussion

3.1. Seasonal Cycle of Surface Ocean pCO_2

[17] Observation of the seasonal cycle of surface ocean pCO_2 over several consecutive years was a major goal of the ANIMATE project. This was partly impaired by the loss of instruments or data which limits data availability to a 614-day period between July 2003 and March 2005. Therein, submergence of the sensor packages from their normal deployment depths of 23–33 m (Table 2) to maximum depths of up to 200 m occurred during certain periods and events. The situation was further aggravated when the mixed layer depth approached the instruments' deployment depths during shallow summer stratification. Some of the data acquired during these times were thus taken below the mixed layer and needed to be excluded from the analysis of the surface ocean pCO_2 cycle. A further possible complication is due to the fact that fixed depth measurements by necessity cannot resolve vertical gradients within the mixed layer, which can occur under high turnover rates. We therefore need to stress the fact that our following analysis is based on the unavoidable assumption that all data measured at a fixed depth within the mixed layer are taken to be representative of the entire mixed layer.

[18] To exclude data which do not represent surface mixed layer conditions, a filter based on SST was used. In the case of the PAP 3 deployment, SST data are available from a T/S sensor installed at 10 m depth underneath a small telemetry float tethered to the subsurface mooring head. When this telemetry float was either not deployed (PAP 2) or lost early into the deployment (PAP 4), remotely sensed microwave SST data were used (AMSR-E, Table 3). The pCO_2 data were considered representative of the mixed layer when the in situ sensor temperature differed by less than 0.3°C and 0.6°C from the SST measured by the 10 m S/T sensor and the satellite-borne microwave instrument, respectively (Figure 3). The temperature criterion was adjusted to allow for measurement error, small-scale variability in mixed layer temperature as well as the scatter associated with the MicroCAT and, more importantly, the AMSR-E temperature data (i.e., width of distribution of temperature residuals). It proved very efficient and mainly eliminated data during summer and early fall periods of high stratification and shallow mixing as evidenced by mixed layer depths estimated from ARGO T/S profiles (Figure 3). Resulting data gaps between mixed layer data were filled by interpolation for all budget and flux calculations.

[19] The emerging picture of the seasonal pCO_2 cycle at the PAP site (Figure 2) shows persistent undersaturation of surface waters by 40 ± 15 μatm (1σ) throughout the year which gives rise to a perennial CO_2 sink (3.2 ± 1.3 mol m^{-2} a^{-1} in 2004, calculated using equation (3)). As expected, this is considerably larger than the annual CO_2 sinks of 1.9 ± 0.2, 1.0 ± 0.1, and 0.05 ± 0.02 mol m^{-2} a^{-1} estimated for subtropical time series at BATS, ALOHA, and ESTOC, respectively [*Gruber et al.*, 2002; *Keeling et al.*, 2004; *González-Dávila et al.*, 2007]. The continuous undersaturation is characteristic of the entire subpolar North Atlantic [*Takahashi et al.*, 2002] and results primarily from the general cooling of surface waters during their passage from low to high latitudes but also results from a comparatively small respiration signal [*Broecker and Peng*, 1992].

[20] On top of this characteristic regional trait, a seasonal pCO_2 cycle is imprinted by the counteracting effects of seasonal warming/cooling, large seasonal changes in the depth of the mixed layer and spring/summer biological activity. As has been shown for this [*Lüger et al.*, 2004] and other subpolar regions [*Takahashi et al.*, 1993, 2002], the decreasing effect on surface ocean pCO_2 of the sizable new production (fueled by wintertime nutrient supply through deep vertical mixing) exceeds the increasing effect of the seasonal warming. The seasonal pCO_2 cycle is therefore characterized by a late summer minimum and late winter maximum, which is the opposite of the situation found at the subtropical time series sites BATS, ALOHA

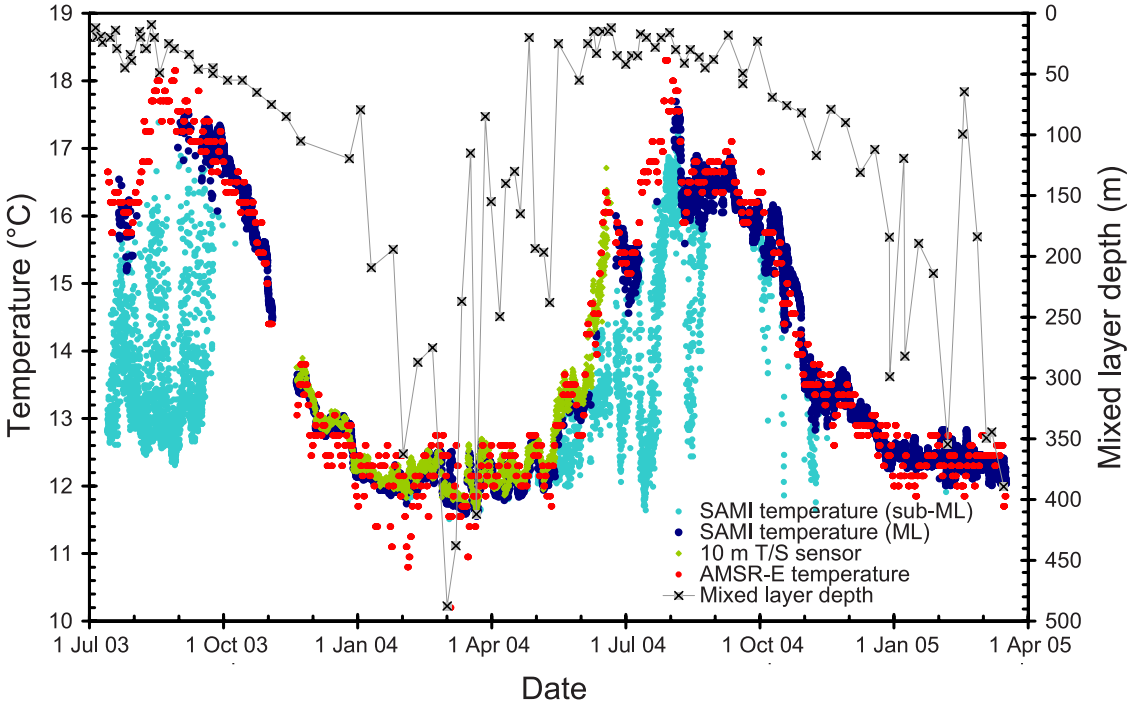

Figure 3. Time series of temperature measured during the course of the PAP 2–4 deployments by (1) the SAMI pCO_2 sensor, (2) a T/S sensor deployed at 10 m depth (PAP 2 only), and (3) the Advanced Microwave Scanning Radiometer on the NASA EOS satellite Aqua. Temperature data of 2 and 3 were used to distinguish mixed layer (ML) and sub-ML locations of the CO_2 sensor. Also shown is mixed layer depth estimated from ARGO float profiles taken within 2° of latitude and longitude of the PAP site.

and ESTOC [*Gruber et al.*, 2002; *Keeling et al.*, 2004; *González-Dávila et al.*, 2007]. An analysis of the physical and biological forcing is provided in section 3.2.

3.2. Physical and Biological Forcing of Surface Ocean pCO_2

[21] We follow a somewhat simplistic but nevertheless instructive way of separating thermal and biological (or more correctly, nonthermal) forcing on surface ocean pCO_2 that has been employed by *Takahashi et al.* [2002]. This approach makes use of the fact that the temperature dependence of pCO_2 under isochemical conditions (i.e., fixed DIC and A_T) is well constrained ($\partial \ln pCO_2/\partial T = 0.04231°C^{-1}$). This allows two measures: (1) construction of the thermally forced seasonal pCO_2 cycle ($pCO_{2,therm}$, equation (1)) removal of the thermal effect from observed pCO_2 ($pCO_{2,nontherm}$, equation (2)):

$$pCO_{2,therm} = \overline{pCO_2} \cdot e^{0.0423 \cdot \left(T_{obs} - \overline{T}\right)} \quad (1)$$

$$pCO_{2,nontherm} = pCO_{2,obs} \cdot e^{0.0423 \cdot \left(\overline{T} - T_{obs}\right)}. \quad (2)$$

[22] In equations (1) and (2), overbars represent annual means and obs stands for observed. Equation (1) perturbs the annual mean pCO_2 (324.6 μatm in 2004) with the observed SST. The resulting $pCO_{2,therm}$ (Figure 4) can be considered as the hypothetical pCO_2 under isochemical conditions, i.e., absence of addition or removal of carbon by biological processes and air-sea exchange. It is a realistic measure of the seasonal thermal forcing on surface ocean pCO_2. In contrast, equation (2) removes this thermal effect on the observed pCO_2 by correcting it to annual mean SST (13.94°C in 2004 based on AMSR-E data). The resulting $pCO_{2,nontherm}$ (Figure 5) represents the observed pCO_2 variability that is not due to thermal effects and must therefore reflect changes in the concentration of DIC and/or A_T. Such changes can be driven by biological carbon fixation and release as well as advection, vertical mixing and air-sea CO_2 transfer. If corrected for the influence of air-sea exchange and restricted to certain reasonably well defined conditions, $pCO_{2,nontherm}$ can be interpreted primarily in terms of biologically mediated carbon changes (section 3.3).

[23] The seasonal range of SST of approximately 5°C translates into a $pCO_{2,therm}$ range of about 70 μatm (Figure 4). The thermally driven winter-to-summer pCO_2 increase of 70 μatm is more than compensated by a decrease of order 120 μatm due to nonthermal factors (Figure 5) causing the observed late summer minimum. Similarly the summer-to-winter cooling effect on pCO_2 is more than compensated by a counteractive chemical influence which causes the observed winter maximum of the seasonal pCO_2 cycle. The seasonal patterns of $pCO_{2,nontherm}$ can be explained qualitatively as a winter-to-summer drop associated with net biological carbon drawdown, i.e., net community production within the mixed layer, and a summer-to-winter increase associated with the deepening of the mixed layer which brings CO_2 from wintertime DIC levels plus a seasonal respiration component back to the surface ocean.

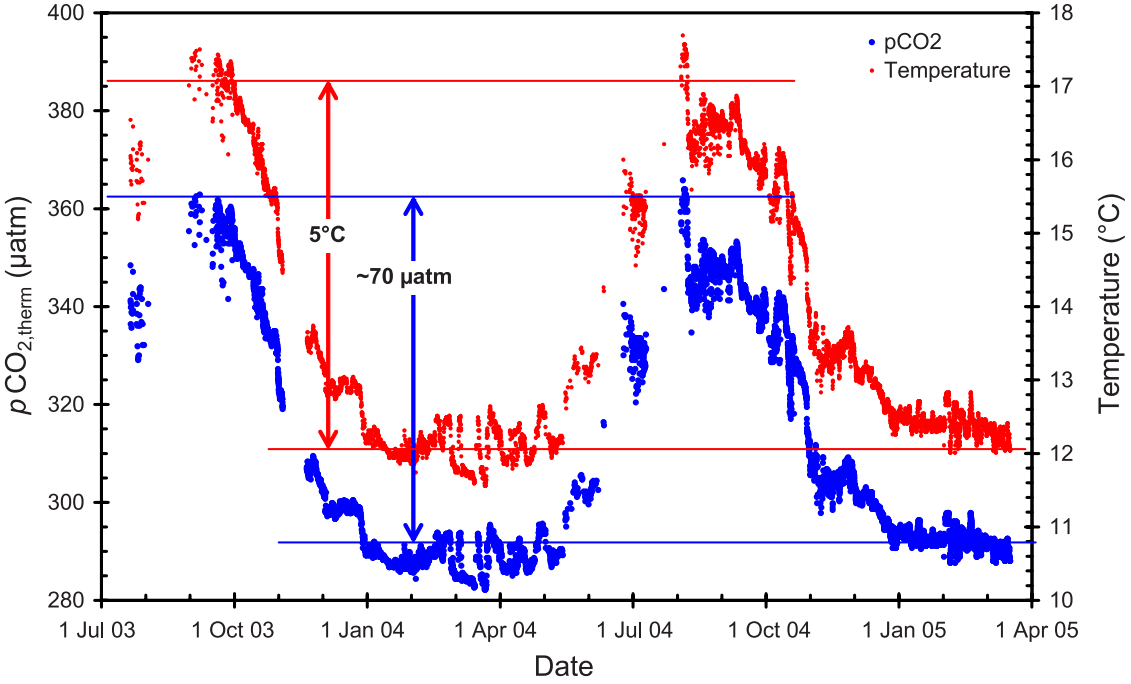

Figure 4. Perturbation of the annual mean pCO_2 (324.6 μatm in 2004) with the observed sea surface temperature (SST). The resulting quantity $pCO_{2,therm}$ (equation (1)) is a measure of the thermal forcing of the seasonal pCO_2 cycle under isochemical conditions in the surface ocean.

3.3. Biological Processes Behind Chemical Signatures

[24] To analyze biological processes, as manifested in the pCO_2 cycle at PAP, in terms of their influence on the inorganic carbon inventory, we calculated the corresponding DIC from $pCO_{2,obs}$ and climatological A_T (Table 3) at in situ temperature. The assumption of conservative behavior for A_T may not be fully valid, especially in heavily calcifying situations such as coccolithophorid blooms. We therefore looked up global 8-day maps showing occurrences of blooms of the coccolithophorid *Emiliania huxleyi*

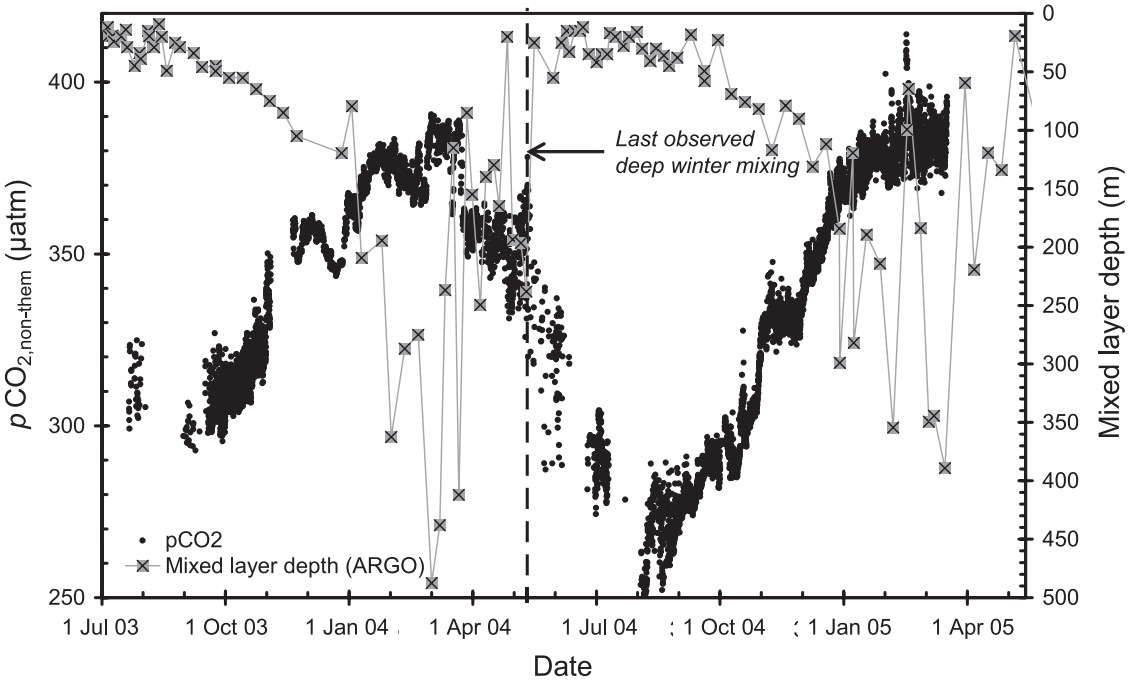

Figure 5. Observed pCO_2 corrected to the annual mean SST of 2004 (13.94°C). The resulting quantity $pCO_{2,nontherm}$ (equation (2)) is a measure of the chemically driven pCO_2 cycle in the surface ocean under isothermal conditions. Also shown are estimated mixed layer depths.

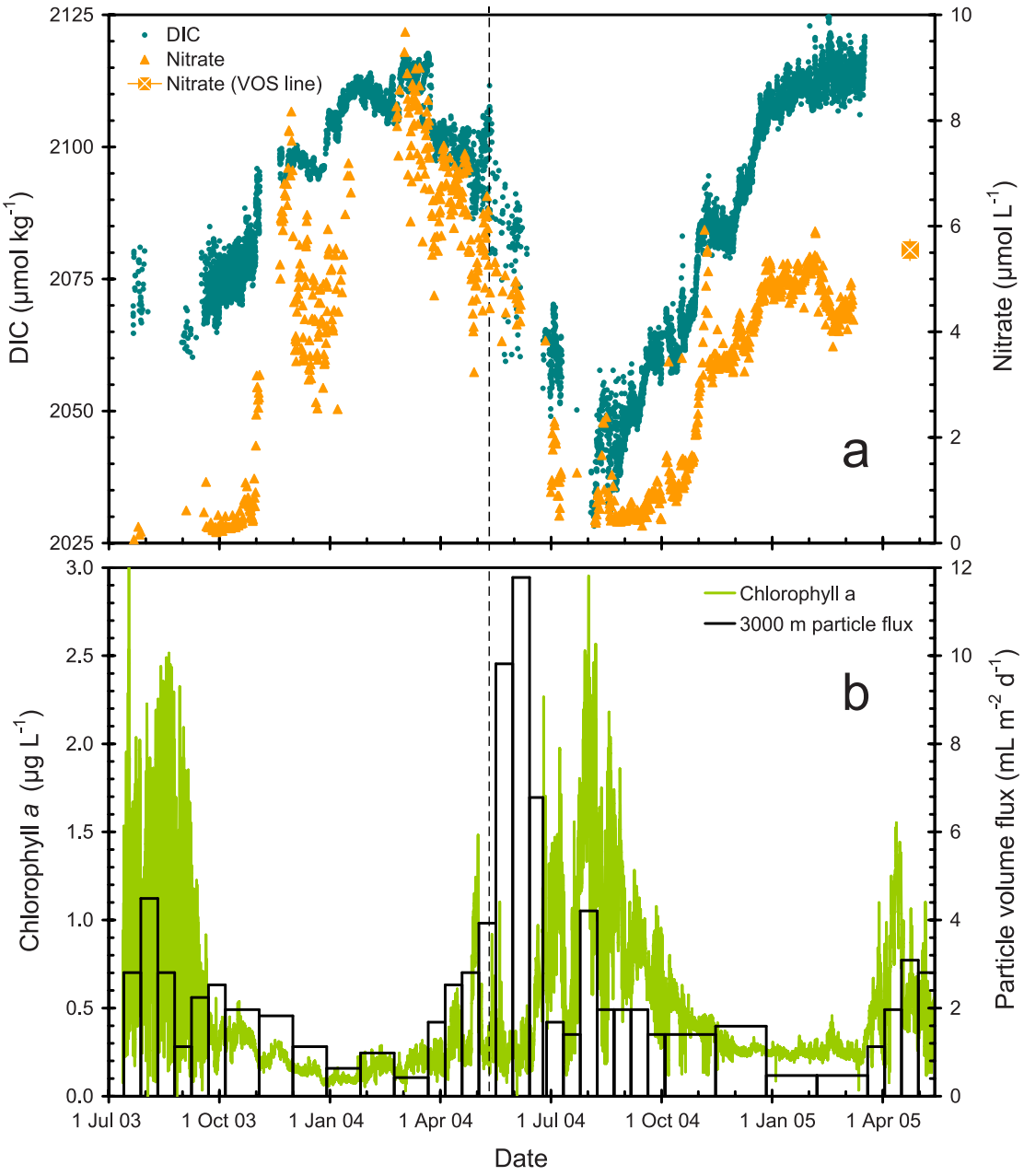

Figure 6. (a) Mixed layer time series of dissolved inorganic carbon concentrations (DIC, left *y*-axis) calculated from observed pCO_2 and climatological total alkalinity and measured nitrate concentrations (right *y*-axis). (b) Mixed layer time series of chlorophyll *a* concentrations (left *y*-axis). Also shown is the particle flux volume at a nominal depth of 3000 m collected by means of a sediment trap at variable sampling intervals (right *y*-axis).

(http://cics.umd.edu/~chrisb/ehux_www.html) that are based on their relatively unique spectral signatures in ocean color imagery of the Sea-viewing Wide Field-of-view Sensor (SeaWiFS). These are based on the original algorithm of *Brown and Yoder* [1994] for Coastal Zone Color Scanner (CSCZ) imagery that has been adapted to SeaWiFS imagery. Maps for the year 2004, to which our present analysis is restricted, show no bloom occurrence at the PAP site. A bloom that was visible more than 4° north of PAP in late July and August 2004 is unlikely to have influenced the PAP site which is located in a region of general eastward surface circulation. The assumption of conservative behavior of surface A_T is therefore justified.

[25] The resulting DIC time series at PAP (Figure 6a) is generated by biological fluxes, vertical entrainment and diffusion, advection, and air-sea exchange. Without information on vertical and horizontal gradients a full mixed layer budget cannot be constructed. A simplified budget calculation is possible, however, under certain assumptions and for restricted periods. First, we assume that the diffusion term is generally small and negligible in this context. Secondly, we assume that the seasonal cycle in the middle

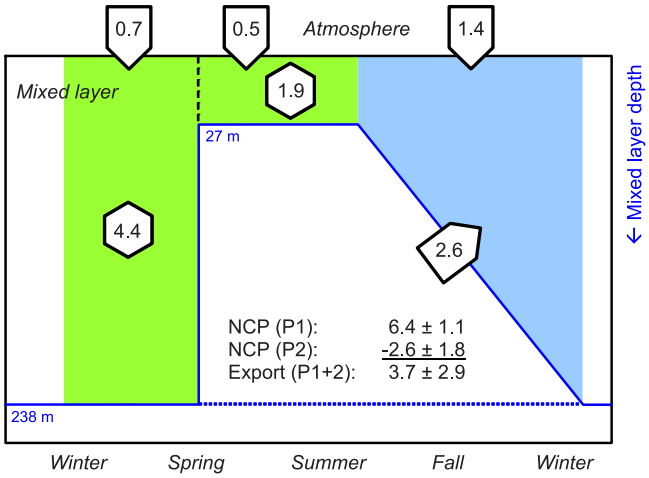

Figure 7. Simplified schematic of the mixed layer carbon budget during periods 1 (green) and 2 (blue), where period 1 is further separated into a pre- and a poststratification part. Arrow-shaped symbols denote boundary fluxes into the mixed layer due to net air-sea transfer of CO_2 and entrainment of DIC. Hexagons stand for the estimated net community production within the mixed layer (corrected for the air-sea CO_2 fluxes shown). All numbers are in units of moles carbon per meters squared during the respective periods.

of this biogeochemical province and remote from major oceanic fronts is generated mainly by local processes and only to a minor extent by advection. Thirdly, during periods of stationary or shoaling mixed layers depths the entrainment term must be zero. In contrast, the CO_2 uptake from the atmosphere during the time series can be quantified reasonably well. For this purpose we produced 8-day averages of air-sea pCO_2 difference (ΔpCO_2), SST, wind speed at 10 m height, and mixed layer depth. We then calculated 8-day CO_2 flux densities, F, using the following bulk equation:

$$F = k \cdot K_0 \cdot \left(pCO_2^{air} - pCO_2^{sea}\right), \quad (3)$$

where k is the transfer coefficient based on the wind speed–dependent formulation of *Nightingale et al.* [2000] scaled to the temperature-dependent Schmidt number according to *Wanninkhof* [1992], K_0 is the CO_2 solubility at in situ T and S after *Weiss* [1974], and pCO_2^{air} and pCO_2^{sea} are the CO_2 partial pressures (at 100% humidity and SST) of air and seawater, respectively. Calculated CO_2 fluxes carry an estimated maximum error of 40% which includes the pCO_2 error as well as the uncertainty in the flux calculation itself (wind speed, transfer coefficient). CO_2 flux densities can be converted into corresponding DIC changes (ΔDIC) when the mixed layer depth (MLD) is known:

$$\Delta\mathrm{DIC} = \frac{F}{\mathrm{MLD}}. \quad (4)$$

[26] DIC changes driven by air-sea exchange range from negligible (<0.02 μmol kg^{-1} d^{-1}) during periods of deep mixing when even large air-sea fluxes were diluted over a large volume of seawater, to a maximum of 0.6 μmol kg^{-1} d^{-1} during times of shallow mixed layers (23 m) and largest ΔpCO_2 (66 μatm).

[27] In the following discussion we define two distinct periods of the seasonal cycle which allow qualitative and quantitative inferences for the 2004 seasonal cycle concerning the net biological productivity and export.

3.3.1. The Productive Season (Period 1)

[28] The productive season (period 1) extended from March (DIC maximum) to early August 2004 (DIC minimum). During this period, inorganic carbon was taken up by net community production (NCP). Nitrate concentrations (Figure 6a) also showed a steady and parallel decline from initial values of 8 to 10 μmol kg^{-1} in March 2004 to values near the limit of detection at about 0.5 μmol kg^{-1} in August 2004. During period 1, mixed layer depths (Figure 5) remained generally deep, with only brief intermittent periods of shallower stratification, until the middle of May when stable shallow stratification (<50 m) suddenly developed and remained until end of September. In a situation of stationary and then shoaling mixed layer depths no vertical entrainment of DIC occurs. If we assume that diffusion across the base of the mixed layer and lateral advection are negligible and if we further correct for uptake of atmospheric CO_2, the DIC and nitrate drawdowns during period 1 can be interpreted as net community production.

[29] The productive period can clearly be separated into a pre- and a poststratification phase. The former ends with a mixed layer depth of 238 m (8-day average) which we adopted as reference depth in the budget calculation. The time and depth integrated DIC (and nitrate) drawdown prior to stratification was calculated for the upper 238 m over nine 8-day intervals starting in March 2004. Fortunately, productivity signals associated with intermittent periods of shallow stratification were redistributed over the 238 m water column at the end of this phase so that they must be reflected in our budget. Furthermore, mixing hardly exceeded a depth of 238 m during this time so detrainment of NCP to below our reference depth should be minimal. During the sharply separated poststratification phase of period 1 we adopted the average mixed layer depth of 27 m as our reference level and performed the time and depth integration over ten 8-day intervals until early August 2004.

[30] The resulting time- and depth-integrated carbon (and nitrate) drawdown within the mixed layer during period 1 (Figure 7) indicates that about two thirds (4.4 ± 0.9 mol C m^{-2}) of the seasonal (mixed layer) NCP of 6.4 ± 1.1 mol C m^{-2} took place before the onset of shallow stratification. We need to point out that this estimate refers to the mixed layer and by necessity misses any production that occurred below in the stratified part of period 1. Additionally the assumption that chemical properties measured at ~23 m depth are representative of the entire mixed layer may be incorrect during periods of deep mixing. Our NCP estimate for the prestratification phase should therefore represent an upper bound while the NCP of the poststratification phase is possibly an underestimate. This reduces the prestratification fraction to <2/3 and brings our estimate in closer agreement with *Garside and Garside* [1993] and *Koeve* [2001] who concluded, for a nearby site (47°N, 20°W), that about half of the spring bloom's total production occurs in advance of stratification. Our mixed layer NCP estimate for March–

August 2004 is 2–3 times larger than the estimates of 3.4 ± 0.8, 2.3 ± 0.8, and 3.3 ± 0.8 mol m^{-2} a^{-1} for the subtropical time series BATS, ALOHA, and ESTOC, respectively [*Gruber et al.*, 2002; *Keeling et al.*, 2004; *González-Dávila et al.*, 2007].

[31] Note that the NCP estimates above are based on relative change in DIC rather than absolute DIC values. Systematic bias would thus be introduced only by a temporal drift in the pCO_2 (and hence DIC) record but not by uncertainty in absolute pCO_2. In our error estimate we assume a maximum uncompensated (by the postcalibration) drift of 2 μatm $month^{-1}$ ($\sim$1 μmol kg^{-1} $month^{-1}$ in DIC). The error estimate further includes a 40% error associated with the air-sea flux estimate. As this correction for net uptake of atmospheric CO_2 accounts for only about 16 ± 6% of the NCP estimate it is of minor significance in the overall error.

[32] It is of interest to explore the timing of the phytoplankton bloom in surface waters and the particle flux as recorded at 3000 m depth (Figure 6b) in the context of mixed layer dynamics. Mixed layer depths (Figure 5) changed rapidly from a deeply mixed winter situation (last observed on 10 May 2004) to a constantly stratified summer situation (first observed on 16 May 2004). Mixed layer chlorophyll *a* concentrations remained moderately elevated ($\sim$0.5 μg L^{-1}) during the first half of the productive cycle and more than doubled afterward during the period with shallower mixed layers (Figure 8a). In fact, a small chlorophyll peak of about 1.5 μg L^{-1} at the end of April coincided with a brief period of shallow stratification ($\sim$20 m). Most of this chlorophyll disappeared when mixing to 200–250 m resumed only a few days later, partly due to dilution but also possibly due to export. In contrast to the concentrations, the mixed layer column-integrated chlorophyll *a* inventory (Figure 8a) dropped from up to 100 mg m^{-2} to values of 10–50 mg m^{-2} after the onset of shallow stratification. This roughly twofold drop in mixed layer chlorophyll is consistent with a twofold drop in the estimated NCP for the two distinct periods before and after stratification (Figure 8b). After stratification and alleviation of light limitation the phytoplankton biomass increased, leading to rapid depletion of available nutrients in the shallow mixed layer to which it was, by then, restricted.

[33] The fate of a major fraction of the biomass produced during the deeply mixed period can be seen quite clearly in the particle volume flux at 3000 m depth (Figure 6b): upon stratification, most of the biomass that was spread over the $\sim$250 m depth range of the final winter mixing was lost. Left behind by the rapidly shoaling mixed layer, it apparently underwent aggregation and transfer to depth within a matter of weeks. A major portion of the annual particle flux thus appears to be mediated by this detrainment mechanism which leads to a strong flux pulse almost immediately following stratification. This pulse was missed in 2003 as sampling only started in mid-July. A small particle flux peak observed in early August (2003 and 2004) probably reflects the point of full exhaustion of macro nutrients and the onset of the decay of the summer phytoplankton biomass.

3.3.2. The Period of Mixed Layer Deepening (Period 2)

[34] Period 1 was followed by a period of deepening mixed layers (40 m to >250 m) between September 2004 and the end of the year during which net productivity in the surface ocean decreased rapidly (Figure 8b) and subsurface DIC was entrained. The entrainment component is a function of preformed DIC levels at the end of the preceding deep mixing period (here in early May 2004) and the NCP that occurred below the mixed layer (and above 238 m) during the period of stratification. While our mixed layer budget completely misses the subsurface NCP component during the second half of period 1, it can be traced by a simple budget calculation. We initialize the budget with the DIC column inventory that is defined by DIC levels at the end of the deep mixing period (May 2004) in the depth range 27–238 m and DIC levels at the end of the stratified part of period 2 for the upper 27 m. We compare this initial DIC inventory with the one found when the preceding mixed layer depth reaches the reference depth of 238 m which occurred at the end of December 2004. When corrected for the atmospheric CO_2 uptake during this time period, any difference between the two inventories should largely reflect the contribution of subsurface NCP (27–238 m) between the onset of stratification and the time when mixing down to 238 m resumed.

[35] Our budget calculation yields an increase in the 238 m column inventory of DIC of 2.6 ± 1.9 mol C m^{-2} which indicates net heterotrophic conditions below the mixed layer and above 238 m during May–December 2004 (Figure 7). The result that across this depth range respiration exceeds production is not surprising and implies that about 40% of the mixed layer NCP accomplished during the period 1 had been respired in the subsurface layer (above 238 m) and was reventilated in the following winter. The remainder of 3.7 ± 3.1 mol C m^{-2} was exported to below the 238 m depth horizon or stored in the (dissolved and particulate) organic carbon pools of the upper 238 m. We believe that the former is largely responsible for the pronounced particle flux peak during period 1 while the latter represents only a small fraction.

[36] NCP estimates restricted to the photic zone would lead to signification overestimation in regions where the maximum mixed layer depth strongly exceeds the depth of the euphotic zone. This is clearly the case at the PAP site and has been demonstrated by *Oschlies and Kähler* [2004] who showed that classical estimates of new production can overestimate biological drawdown over an annual cycle by 30–50% in the subpolar northeast Atlantic Ocean (50°–62°N) by ignoring the wintertime reventilation of seasonally accumulated respiratory CO_2.

[37] Our carbon budget for the upper 238 m is not closed for three reasons. First, our budget only covers a 9-month period and may therefore miss important fluxes that occur during the other three months. Secondly and most importantly, the annual cycle in 2004/2005 itself is not fully closed as nitrate levels by March 2005 ($\sim$5 μmol kg^{-1}) had not resumed the high levels (>8 μmol kg^{-1}) that were seen 1 year before. This certainly has to do with the fact that winter mixing reached significantly deeper in 2004 than in 2005. Finally, our carbon fluxes carry significant error which preclude firm statement on overall budget closure.

3.4. C:N Stoichiometry of Biological Signals

[38] Figure 6a invites to explore the C:N stoichiometry of biological processes as reflected in the DIC and nitrate changes. At first sight, C:N stoichiometries of periods 1 and

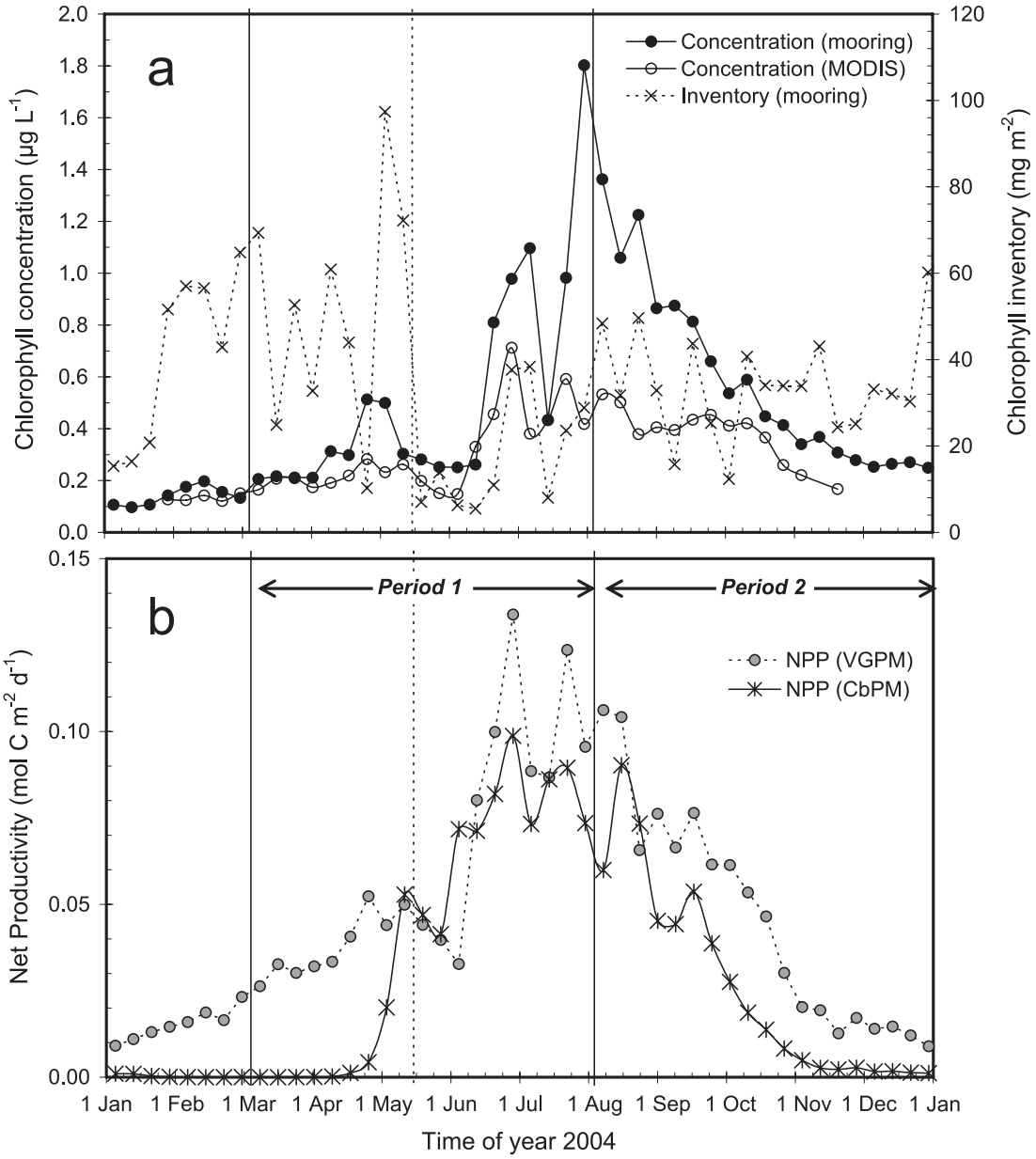

Figure 8. (a) Chlorophyll concentration (left *y*-axis) and inventory (right *y*-axis) in the mixed layer as observed at the PAP mooring during 2004 (8-day averages). For comparison, the remotely sensed chlorophyll concentration from the Moderate-Resolution Imaging Spectroradiometer sensor is shown (averages of 16 pixels around the PAP site from the 1080 × 2160 global grid). The productive period of net carbon drawdown (period 1) is indicated by vertical lines. The dashed vertical line marks the onset of shallow stratification. (b) Estimates of net primary production using two satellite-based approaches (see text for further details).

2 appear to be markedly different: While the period 1 DIC decrease is followed by a DIC increase of similar magnitude during period 2, the nitrate increase of period 2 accounts for just over half of the decrease during period 1. This picture of nonmatching stoichiometries of net community production and respiration is misleading, however, due to the biasing effect of unidirectional air-sea transfer of CO_2 during both periods. As a consequence, the NCP-driven carbon drawdown in the mixed layer during period 1 is larger than the observed DIC decrease whereas the net respiration signal seen during period 2 is smaller than indicated by the observed DIC increase. Thus for an unbiased determination of C:N ratios, DIC values corrected for the air-sea exchange component have to be used (Figure 9).

[39] The stoichiometric ratio of the carbon and nitrate drawdown during period 1 was 11.0 ± 0.7 (model II regression of corrected DIC versus nitrate). This is significantly greater than the canonical Redfield value of around 7 [e.g., *Redfield et al.*, 1963; *Anderson and Sarmiento*, 1994; *Körtzinger et al.*, 2001a] and indicative of the phenomenon

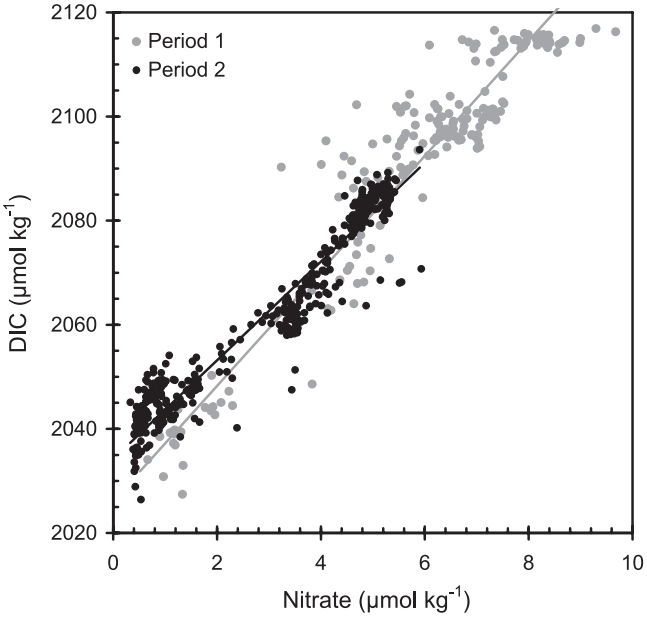

Figure 9. Relationship between DIC, corrected for the air-sea exchange component, and nitrate during periods 1 and 2.

of carbon overconsumption [*Toggweiler*, 1993] that has been observed on various occasions [*Sambrotto et al.*, 1993], especially toward the end of the productive season [*Körtzinger et al.*, 2001b; *Koeve*, 2004] when the system runs into nitrate stress. The return flux of respired DIC and nitrate during period 2 occurs with a C:N ratio of 9.5 ± 0.3 which is fairly close to the signature of production and also significantly higher than the classical Redfield value (Figure 9). Carbon overconsumption therefore not only shows up in the carbon and nitrate uptake ratios of NCP but is also evident in the ratios at which carbon and nitrogen are released during respiration and returned to the mixed layer during deep winter mixing.

3.5. Comparison of Productivity Estimates

[40] We estimated a seasonal mixed layer NCP of 6.4 ± 1.1 mol C m^{-2} for period 1 in 2004 which can be apportioned into a prestratification (4.4 ± 0.9 mol C m^{-2}) and a poststratification component (1.9 ± 0.3 mol C m^{-2}). Since it is referenced to the mixed layer this estimate does not include sub mixed layer NCP that occurs above the reference depth of 238 m during the stratified period. Our inventory calculation at the end of period 2 reveals, however, that net buildup of DIC occurred below the mixed layer and above 238 m between May and December 2004. This negative NCP of 2.6 ± 1.8 mol C m^{-2} is due to net respiration of (particulate and dissolved) organic matter which is reventilated to the surface ocean during deep winter mixing. The residual annual NCP of 3.8 ± 2.9 mol C m^{-2} represents the fraction of the seasonal NCP that has been exported to depths > 238 m. This depth horizon falls somewhat short of the maximum winter mixed layer depths for which in steady state full budget closure over decadal timescales would be expected.

[41] It is of interest to compare our NCP estimates with other productivity products. Prominent global productivity estimates derived from satellite imagery provide estimates of net primary production (NPP), i.e., the difference between gross primary production (GPP) and autotrophic respiration, and therefore exclude the heterotrophic respiration that is included in our NCP estimates. These products, however, are referenced to the euphotic zone depth rather than mixed layer depth which precludes a direct comparison. This is particularly true for the NCP estimate for the second half of period 1 which is restricted to a rather shallow mixed layer of on average 27 m and hence misses sub mixed layer production. A meaningful comparison is therefore restricted to the timing aspect of productivity as documented in the various products.

[42] We used NPP estimates based on two different methods: (1) remotely sensed chlorophyll concentrations and a light-dependent, depth-resolved model for carbon fixation (Vertically Generalized Production Model (VGPM) [*Behrenfeld and Falkowski*, 1997]) and (2) a more recent approach based on remotely sensed chlorophyll concentrations and particulate backscattering coefficients (Carbon-Based Production Model (CbPM) [*Behrenfeld et al.*, 2005]). Both methods use the same chlorophyll data and parameterizations for the light dependence and euphotic zone depth. Cumulative NPP values for period 1 + 2 (averages of 6 pixels around the PAP site from the 540 × 1080 global grid) are 16.3 mol C m^{-2} a^{-1} (VGPM) and 10.4 mol C m^{-2} a^{-1} (CbPM). The only information that is of use in this context is that NPP estimates are larger than our NCP estimate which by necessity has to be the case. A closer inspection of the timing of the NPP estimates (Figure 8b) reveals major discrepancies between the VGPM and CbPM methods in the deeply mixed first half of period 1. In addition, both are significantly smaller than our NCP estimate for this period. Although our approach tends to overestimate NCP during this particular period, the occurrence of a pronounced particle flux peak right the onset of stratification and before the development of a surface phytoplankton bloom provides clear evidence that the NPP estimates (particularly CbPM) miss a major signal during the period of deep mixed layers. This may be due to the fact that the remotely sensible optical properties employed in the calculation of chlorophyll and backscatter are restricted to the upper water column which would cause greatest biases during periods of mixing.

[43] Given the major mismatch between NPP and NCP in the early deeply mixed part of season it is of interest to pose the question how the prestratification productivity which is seen so clearly in the chemical data reconciles with the critical depth theory of *Sverdrup* [1953]. *Obata et al.* [1996] showed that aphotic conditions (i.e., mixed layer depth > critical depth) prevail in the subpolar North Atlantic until April/May, when the increase of insolation and the decrease in mixed layer depth cause a change to euphotic conditions. According to the theory this is the trigger for exponential increase in phytoplankton biomass. Our data show that the transition from aphotic to euphotic occurred during the second week of May 2004. However, apart from a small chlorophyll peak immediately afterward, the major increase in phytoplankton biomass (or more correctly chlorophyll concentrations) did not occur until more than one month later. This indicates that additional factors must exist that trigger phytoplankton blooms in the region. Our data do not

provide further insight into these which leaves the issue open to speculation ranging from transient iron depletion to internal ecological mechanisms. On the other hand, moderate peaks in phytoplankton biomass are seen before the onset of stratification, i.e., during a period when according to the critical depth theory no net community production should occur.

[44] There are several lines of reasoning to resolve this apparent contradiction. First, the critical depth concept assumes vertically constant community respiration. As pointed out by *Smetacek and Passow* [1990], some algae are capable of growing under extremely low light levels indicating that the depth of the euphotic zone and hence the position of the compensation depth may have been underestimated. If we further take into account that the zooplankton community may still partly be in a dormant mode, we may conclude that community respiration in the early prestratification stage of the productive cycle may be considerably smaller than typical depth-independent values used in the classical critical depth concept [e.g., *Sverdrup*, 1953; *Obata et al.*, 1996]. For example, a moderate twofold decrease of the respiration level from 10% to 5% of maximal photosynthetic rate will caused a doubling of the critical depth. Since respiration may be suppressed by more than a factor of 2 and community level respiration may vary at least by a factor of 10 [*Siegel et al.*, 2002] the critical depth is not constrained well under these circumstances.

[45] Therefore, a further aspect that needs be looked at in this context is the timescale of vertical mixing in the surface mixed layer in relation to the timescale of exponential phytoplankton growth. The view of a rapidly and more or less continuously mixed surface layer is clearly too simple. In reality the timescale of vertical mixing may range from days to a few weeks depending on the physical environment allowing for transient periods of partial stratification and development of vertical gradients. Under such conditions, phytoplankton species having not only responded to the necessity of lowering their respiration but having also developed the capability of rapid growth will experience a competitive advantage. So even if vertical homogenization occurs repeatedly during the prestratification period, local physical conditions may still allow for transient periods of more favorable conditions and enhanced productivity by fast responding bloom species. In addition to the respiration aspect such a more dynamic picture would also explain the observed net community production during times when it should be absent according to the classical Sverdrup concept.

4. Conclusions

[46] The 2-year time series analyzed in this study represents a significant effort by a multinational European consortium. With present technology, the generation of such long-term biogeochemical time series for the surface ocean remains a very demanding task, particularly because the instruments, platforms, and methods are still under development. Data losses due to failure or loss of instruments/moorings cannot always be avoided and data gaps for certain parameters at certain times limit the interpretation of the data. The 2-year record shown here represents that part of a 4-year effort for which the highest simultaneous data return was achieved.

[47] When successful, these efforts deliver unique multiparameter data sets that provide most valuable and unique insight into physical-biogeochemical coupling and the characteristics of ocean productivity and carbon export. On the basis of our analysis the following conclusions can be drawn for the PAP site (49°N/16.5°W) that we believe are representative of Longhurst's NADP, a region hosting one of the most prominent spring blooms in the global ocean.

[48] 1. On the annual timescale, the surface ocean in this region acts as a perennial sink for atmospheric CO_2. In 2004, this was estimated at 3.2 ± 1.3 mol m^{-2} a^{-1} which is indistinguishable from the climatological flux of 3.3 mol m^{-2} a^{-1} for the pixel centered at 48°N/17.5°W according to *Takahashi et al.* [2002]. This feature, which the region shares with most of the subpolar North Atlantic, is mainly a consequence of the cooling of surface waters on their transit from low to high latitudes as they travel with the North Atlantic Drift.

[49] 2. The seasonal pCO_2 cycle around the general moderate undersaturation (see above) is characterized by a marked summer minimum (winter maximum). The effect of summertime biological carbon drawdown on pCO_2 exceeds the counteracting effect of the seasonal SST cycle (hence the summer pCO_2 minimum). This is typical of subpolar regions and in contrast to the situation in the subtropics [*Takahashi et al.*, 2002; *Lüger et al.*, 2004]. Deviations from the seasonal cycle of climatological pCO_2 can be as large as 40 μatm;

[50] 3. The surface ocean system shows a rapid change from deep winter mixing to shallow summer stratification which has major consequences for biological production. At the appearance of summer stratification most of the phytoplankton biomass that has already accumulated at this time is detrained from the mixed layer and subsequently subjected to particle aggregation and deep export to depth;

[51] 4. According to our analysis up to two thirds of the seasonal mixed layer net community production during the productive season were accomplished before the onset of shallow summer stratification. Low levels of community respiration as well as transient periods of favorable environmental conditions may explain the observed existence of prestratification productivity in a setting where the classical critical depth theory of *Sverdrup* [1953] provides little possibility for substantial NCP. At the PAP site, Sverdrup's critical depth concept appears too static to understand and predict the observed dynamics.

[52] 5. We provide further evidence that the phenomenon of carbon overconsumption may be a typical feature of the subpolar northeast Atlantic as it shows up in the chemical signatures of net community production and respiration;

[53] 6. Seasonal sub mixed layer accumulation of respiratory CO_2 in the upper 238 m of the water column was found to be an important factor and accounted for slightly more than one third of carbon drawdown mediated by NCP during the productive season. The remainder is assumed to have been exported to depths >238 m.

[54] 7. Biological productivity in subpolar oceans exhibits a very dynamic character that is intimately coupled to the dynamics of the mixed layer. From a carbon budget perspective, the base of the winter mixed layer is certainly a

better reference horizon for productivity estimates than the base of the euphotic zone. Future development of satellite-based algorithm should try to take this into account.

[55] The dynamics of biologically mediated carbon export from the surface ocean are important aspects of the carbon cycle. The effect of future climate change on biological production in the ocean will be mediated to a major extent by changes in the physical environment. Reliable predictions will thus only be possible if the consequences of changes in environmental factors such as stratification and mixed layer depth are adequately reflected. The results from this long-term effort at the PAP site may help to develop, constrain, and test the implementation of these factors in models and forecasts.

[56] **Acknowledgments.** We would like to acknowledge the major efforts and skills of the various ship crews and scientific parties who prepared, deployed, recovered, and refurbished the multidisciplinary moorings at the PAP long-term ocean observatory. We are grateful to Maureen Pagnani for management of the ANIMATE data. We thank Cory Beatty (Department of Chemistry, University of Montana, Missoula) for quality checks of the SAMI pCO_2 data. We also thank Robert O'Malley (Department of Botany and Plant Pathology, Oregon State University, Corvallis) for providing the VGPM and CbPM productivity estimates as well as MODIS chlorophyll data for the PAP site. Finally, our thanks are due to two anonymous reviewers, whose insightful and thorough comments helped to improve the manuscript significantly. This work was funded by the European Commission through the 5th framework project ANIMATE (Ref. EVR1-CT-2001-40014, 2002–2004) and 6th framework integrated project MERSEA (Ref. 502885, 2004–2008). This article was written during a sabbatical of the first author (A.K.) at the School of Oceanography, University of Washington, Seattle, for which he is very grateful to his host, Paul Quay.

References

Anderson, L. A., and J. L. Sarmiento (1994), Redfield ratios of remineralization determined by nutrient data analysis, *Global Biogeochem. Cycles*, *8*, 65–80.

Behrenfeld, M. J., and P. G. Falkowski (1997), Photosynthetic rates derived from satellite-based chlorophyll concentration, *Limnol. Oceanogr.*, *42*, 1–20.

Behrenfeld, M. J., E. Boss, D. A. Siegel, and D. M. Shea (2005), Carbon-based ocean productivity and phytoplankton physiology from space, *Global Biogeochem. Cycles*, *19*, GB1006, doi:10.1029/2004GB002299.

Broecker, W. S., and T.-H. Peng (1992), Interhemispheric transport of carbon dioxide by ocean circulation, *Nature*, *356*, 587–589.

Brown, C. W., and J. A. Yoder (1994), Coccolithophorid blooms in the global ocean, *J. Geophys. Res.*, *99*, 7467–7482.

de Boyer Montégut, C., G. Madec, A. S. Fischer, A. Lazar, and D. Iudicone (2004), Mixed layer depth over the global ocean: An examination of profile data and a profile-based climatology, *J. Geophys. Res.*, *109*, C12003, doi:10.1029/2004JC002378.

DeGrandpre, M. D., T. R. Hammar, S. P. Smith, and F. L. Sayles (1995), In situ measurements of seawater pCO_2, *Limnol. Oceanogr.*, *40*, 969–975.

DeGrandpre, M. D., M. M. Baehr, and T. R. Hammar (1999), Calibration-free optical chemical sensors, *Anal. Chem.*, *71*, 1152–1159.

Dickson, A. G., and F. J. Millero (1987), A comparison of the equilibrium constants for the dissociation constants of carbonic acid in seawater media, *Deep Sea Res.*, *34*, 1733–1743.

Garside, C., and J. C. Garside (1993), The "f-ratio" on 20°W during the North Atlantic Bloom Experiment, *Deep Sea Res., Part II*, *40*, 75–90.

GLOBALVIEW-CO_2 (2006), Cooperative Atmospheric Data Integration Project—Carbon dioxide, report, NOAA GMD, Boulder, Colo.

González-Dávila, M., J. M. Santana-Casiano, and E. F. González-Dávila (2007), Interannual variability of the upper ocean carbon cycle in the northeast Atlantic Ocean, *Geophys. Res. Lett.*, *34*, L07608, doi:10.1029/2006GL028145.

Gruber, N., C. D. Keeling, and N. R. Bates (2002), Interannual variability in the North Atlantic Ocean carbon sink, *Science*, *298*, 2374–2378.

Johnson, K. M., K. D. Wills, D. B. Butler, W. K. Johnson, and C. S. Wong (1993), Coulometric total carbon dioxide analysis for marine studies: Maximizing the performance of an automated gas extraction system and coulometric detector, *Mar. Chem.*, *44*, 167–187.

Keeling, C. D., H. Brix, and N. Gruber (2004), Seasonal and long-term dynamics of the upper ocean carbon cycle at Station ALOHA near Hawaii, *Global Biogeochem. Cycles*, *18*, GB4006, doi:10.1029/2004GB002227.

Koeve, W. (2001), Wintertime nutrients in the North Atlantic—New approaches and implications for new production estimates, *Mar. Chem.*, *74*, 245–260.

Koeve, W. (2004), Spring bloom carbon to nitrogen ratio of net community production in the temperate N. Atlantic, *Deep Sea Res., Part I*, *51*, 1579–1600.

Körtzinger, A., J. I. Hedges, and P. D. Quay (2001a), Redfield ratios revisited: Removing the biasing effect of anthropogenic CO_2, *Limnol. Oceanogr.*, *46*, 964–970.

Körtzinger, A., W. Koeve, P. Kähler, and L. Mintrop (2001b), C:N ratios in the mixed layer during the productive season in the northeast Atlantic Ocean, *Deep Sea Res., Part I*, *48*, 661–688.

Lampitt, R. S., B. J. Bett, K. Kiriakoulakis, E. E. Popova, O. Ragueneau, A. Vangriesheim, and G. A. Wolff (2001), Material supply to the abyssal seafloor in the Northeast Atlantic, *Prog. Oceanogr.*, *50*, 27–63.

Lee, K., L. T. Tong, F. J. Millero, C. L. Sabine, A. G. Dickson, C. Goyet, G.-H. Park, R. Wanninkhof, R. A. Feely, and R. M. Key (2006), Global relationships of total alkalinity with salinity and temperature in surface waters of the world's oceans, *Geophys. Res. Lett.*, *33*, L19605, doi:10.1029/2006GL027207.

Lewis, E., and D. W. R. Wallace (1998), Program developed for CO_2 system calculations, *Rep. ORNL/CDIAC-105*, Carbon Dioxide Infor. Anal. Cent., Oak Ridge Natl. Lab., U.S. Dept. of Energy, Oak Ridge, Tenn.

Longhurst, A. R. (2007), *Ecological Geography of the Sea*, 2nd ed., 542 pp., Academic, Boston, Mass.

Lüger, H., D. W. R. Wallace, A. Körtzinger, and Y. Nojiri (2004), The pCO_2 variability in the midlatitude North Atlantic Ocean during a full annual cycle, *Global Biogeochem. Cycles*, *18*, GB3023, doi:10.1029/2003GB002200.

Mehrbach, C., C. H. Culberson, J. E. Hawley, and R. M. Pytkowicz (1973), Measurement of the apparent dissociation constants of carbonic acid in seawater at atmospheric pressure, *Limnol. Oceanogr.*, *18*, 897–907.

Mintrop, L., F. F. Pérez, M. González-Davila, J. M. Santana-Casiano, and A. Körtzinger (2000), Alkalinity determination by potentiometry: Intercalibration using three different methods, *Cienc. Mar.*, *26*, 23–37.

Nightingale, P. D., G. Malin, C. S. Law, A. J. Watson, P. S. Liss, M. I. Liddicoat, J. Boutin, and R. C. Upstill-Goddard (2000), In situ evaluation of air-sea gas exchange parameterizations using novel conservative and volatile tracers, *Global Biogeochem. Cycles*, *14*, 373–387.

Obata, A., J. Ishizaka, and M. Endoh (1996), Global verification of critical depth theory for phytoplankton bloom with climatological in situ temperature and satellite ocean color data, *J. Geophys. Res.*, *101*, 20,657–20,667.

Oschlies, A., and P. Kähler (2004), Biotic contribution to air-sea fluxes of CO_2 and O_2 and its relation to new production, export production, and net community production, *Global Biogeochem. Cycles*, *18*, GB1015, doi:10.1029/2003GB002094.

Redfield, A. C., B. H. Ketchum, and F. A. Richards (1963), The influence of organisms on the composition of sea water, in *The Sea*, edited by M. N. Hill, pp. 26–77, Interscience, New York.

Sambrotto, R. N., G. Savidge, C. Robinson, P. Boyd, T. Takahashi, D. M. Karl, C. Langdon, D. Chipman, J. Marra, and L. Codispoti (1993), Elevated consumption of carbon relative to nitrogen in the surface ocean, *Nature*, *363*, 248–250.

Siegel, D. A., S. C. Doney, and J. A. Yoder (2002), The North Atlantic spring phytoplankton bloom and Sverdrup's critical depth hypothesis, *Science*, *296*, 730–733.

Smetacek, V., and U. Passow (1990), Spring bloom initiation and Sverdrup's critical-depth model, *Limnol. Oceanogr.*, *35*, 228–234.

Steinberg, D. K., C. A. Carlson, N. R. Bates, R. J. Johnson, A. F. Michaels, and A. H. Knap (2001), Overview of the US JGOFS Bermuda Atlantic Time-Series Study (BATS): A decade-scale look at ocean biology and biogeochemistry, *Deep Sea Res., Part II*, *48*, 1405–1447.

Sverdrup, H. U. (1953), On conditions for the vernal blooming of phytoplankton, *J. Conseil Exp. Mer.*, *18*, 287–295.

Takahashi, T., J. Olafsson, J. Goddard, D. W. Chipman, and S. C. Sutherland (1993), Seasonal variation of CO_2 and nutrients in the high-latitude surface oceans: A comparative study, *Global Biogeochem. Cycles*, *7*, 843–878.

Takahashi, T., et al. (2002), Global air-sea CO_2 flux based on climatological surface ocean pCO_2, and seasonal biological and temperature effects, *Deep Sea Res., Part II*, *49*, 1601–1622.

Toggweiler, J. R. (1993), Oceanography—carbon overconsumption, *Nature*, *363*, 210–211.

Wanninkhof, R. (1992), Relationship between wind speed and gas exchange over the ocean, *J. Geophys. Res.*, *97*, 7373–7382.

Weiss, R. F. (1974), Carbon dioxide in water and seawater: The solubility of a non-ideal gas, *Mar. Chem.*, *2*, 203–215.

Wentz, F., and T. Meissner (2004), AMSR-E/Aqua daily L3 global ascending/descending 0.25° × 0.25° ocean grids V001, March to June 2004, http://www.nsidc.org/data/ae_dyocn.html, Natl. Snow and Ice Data Cent., Boulder, Colo.

M. D. DeGrandpre, Department of Chemistry, University of Montana, Missoula, MT 59812, USA.

S. Hartman and R. S. Lampitt, Ocean Biogeochemistry and Ecosystems Research Group, National Oceanography Centre, Southampton SO14 3ZH, UK.

J. Karstensen, A. Körtzinger, and D. W. R. Wallace, Leibniz-Institut für Meereswissenschaften (IFM-GEOMAR), Kiel D-24015, Germany. (akoertzinger@ifm-geomar.de)

O. Llinás and M. G. Villagarcia, Instituto Canario de Ciencias Marinas, Telde, Gran Canaria E-35200, Spain.

U. Send, Scripps Institution of Oceanography, University of California, San Diego, La Jolla, CA 92093, USA.